
Calibrated Similarity for Reliable Geometric Analysis of Embedding Spaces

A Human-Aligned Metric for Interpretable Similarity Measurement

Nicolas Tacheny
 University of Mons (Mons, Belgium)
 nicolas.tacheny@gmail.com

Abstract

While raw cosine similarity in pretrained embedding spaces exhibits strong rank correlation with human judgments, anisotropy induces systematic miscalibration of absolute values: scores concentrate in a narrow high-similarity band regardless of actual semantic relatedness, limiting interpretability as a quantitative measure. Prior work addresses this by modifying the embedding space (whitening, contrastive fine-tuning), but such transformations alter geometric structure and require recomputing all embeddings.

Using isotonic regression trained on human similarity judgments, we construct a monotonic transformation that achieves near-perfect calibration ($ECE \approx 0$, $MBE = 0$) while preserving rank correlation (Spearman $\rho = 0.856$) and local stability (98% across seven perturbation types). Our contribution is not to replace cosine similarity, but to restore interpretability of its absolute values through monotone calibration, without altering its ranking properties.

We characterize isotonic calibration as an order-preserving reparameterization and prove that all order-based constructions—angular ordering, nearest neighbors, threshold graphs and quantile-based decisions—are invariant under this transformation.

1 Introduction

Cosine similarity is the standard metric for comparing vectors in semantic embedding spaces. While it exhibits strong rank correlation with human judgments, *anisotropy*—vectors concentrate in a narrow cone rather than distributing uniformly across the hypersphere [1]—induces systematic miscalibration of absolute values, which cluster in a narrow high-value band even for semantically distant pairs.

The problem. This observation does not contradict the strong empirical performance of cosine similarity in ranking tasks; rather, it highlights a mismatch between relative ordering and absolute interpretability. When absolute values matter—threshold-based decisions, clustering, cross-model comparison—miscalibration has fundamental consequences. A threshold of 0.8 has no consistent semantic interpretation across models or datasets. Clustering algorithms may merge semantically distinct groups when all pairs appear highly similar. The issue is not that cosine similarity fails, but that its *absolute values lack interpretability* as a quantitative measure of semantic relatedness.

Why this matters. Without calibration, the geometry of embedding spaces exists but absolute measurements are not interpretable. Similarities can be computed, but their values carry no consistent meaning across contexts. This is analogous to using an uncalibrated thermometer: it preserves ordering (hotter vs. colder) but its readings cannot be compared across instruments or used for

absolute judgments. For applications requiring interpretable absolute values, calibration is a *necessary condition*.

Existing approaches and their limitations. Prior work addresses anisotropy by modifying the embedding space itself. Su et al. [2] proposed whitening transformations to decorrelate embeddings. Contrastive learning methods [3] improve uniformity through fine-tuning. However, these approaches have significant drawbacks: they alter the geometric structure of the space, require recomputing all embeddings and may affect properties beyond similarity (e.g., linear separability for classification).

Our approach: calibrate the metric, not the space. We propose a fundamentally different solution. Instead of transforming embeddings, we *calibrate the similarity metric itself*. Using human similarity judgments as ground truth, we learn a monotonic transformation that maps raw cosine scores to human-aligned values. This post-processing approach preserves the embedding space intact while restoring measurement interpretability. *Human-aligned* here refers to statistical alignment with empirical human similarity judgments, not to any claim of semantic optimality or universality.

Contributions. This work is not about introducing a new calibration algorithm—isotonic regression is well-established [4]. Our contribution is a theoretical characterization of similarity calibration as a validity condition for geometric analysis. To our knowledge, this is the first work to formalize calibration as a validity condition for similarity-based geometric analysis in embedding spaces:

1. **Miscalibration of absolute values.** We demonstrate empirically that while raw cosine similarity preserves ranking, its absolute values are systematically miscalibrated due to anisotropy, limiting interpretability for threshold-based decisions and cross-model comparison.
2. **Empirical validation.** We validate that isotonic calibration achieves near-perfect alignment with human judgments ($ECE \approx 0$, $MBE = 0$) while preserving local stability (98% across seven perturbation types).
3. **Structural invariance under calibration.** We characterize isotonic calibration as an order-preserving reparameterization and prove that angular ordering, nearest-neighbor relations, threshold graphs and quantile-based thresholds are invariant under this transformation.
4. **Probabilistic coherence.** We derive statistically grounded similarity thresholds from human judgment distributions, with provable preservation of confidence guarantees under calibration.

Paper organization. Section 2 positions our work relative to embedding geometry and calibration literature. Section 3 defines the semantic embedding space. Section 4 analyzes similarity distributions and quantifies the model-human alignment gap. Section 5 presents calibration methods and empirical results. Section 6 establishes the structural invariants preserved under calibration. Section 7 validates local stability empirically. Section 8 discusses applications. Section 9 concludes.

2 Related Work

Embedding anisotropy: the problem. Ethayarajh [1] demonstrated that contextualized representations from BERT, ELMo and GPT-2 become increasingly anisotropic in upper layers: vectors cluster in a narrow cone, causing high cosine similarities even between semantically distant items. Gao et al. [5] termed this the “representation degeneration problem.” Wang and Isola [3] formalized the issue through alignment-uniformity analysis: pretrained embeddings achieve alignment (similar items close) but violate uniformity (vectors not spread across the hypersphere).

Existing solutions: modifying the embedding space. Prior approaches address anisotropy by transforming the embedding space itself. Su et al. [2] proposed whitening to decorrelate and

normalize embeddings. Contrastive fine-tuning methods improve uniformity through additional training [3]. These approaches share a common limitation: they modify the representation space, requiring recomputation of all embeddings and potentially altering geometric properties beyond similarity.

Calibration in machine learning. Calibration aligns model outputs with ground truth distributions. Platt [6] introduced sigmoid calibration for SVMs. Zadrozny and Elkan [4] showed isotonic regression effectively calibrates classifier probabilities. Niculescu-Mizil and Caruana [7] systematically compared methods, finding isotonic regression robust across classifiers. Guo et al. [8] revealed that modern neural networks are poorly calibrated despite high accuracy. Desai and Dur-ratt [9] extended this analysis to pretrained transformers.

All prior calibration work targets *classification confidence*. We extend the paradigm to *semantic similarity*, using human judgments as calibration targets.

Semantic similarity benchmarks. The STS Benchmark [10] provides human-annotated sentence pairs with graded similarity scores. MTEB [11] extends evaluation across embedding tasks. These datasets evaluate embedding quality but have not been used for similarity calibration.

Gap addressed by this work. Two research threads have developed independently: (1) characterizing and correcting embedding anisotropy through space transformations [1, 2, 3], and (2) calibrating model outputs against ground truth [7, 8]. No prior work connects these threads by applying calibration to semantic similarity.

Our contribution is this connection: we show that calibration techniques developed for classifier confidence transfer directly to similarity metrics, providing a lightweight post-processing solution that achieves human alignment without modifying embeddings. This is practically significant because it works with any pretrained model, requires no retraining and preserves all geometric properties of the original space.

3 Semantic Embedding Space

3.1 Embedded Object Space

Before defining how we measure semantic similarity, we must first specify what is being measured. We consider *embedded objects*: entities that can be represented as vectors in the representation space and compared for semantic similarity. While embedded objects can take various modalities (text, images, audio, code, etc.), in this paper we focus exclusively on **textual objects**.

We define the **object space** \mathcal{A} as the set of all possible text strings. Each element $a \in \mathcal{A}$ represents a complete textual unit.

While \mathcal{A} is finite (bounded by the model’s vocabulary and maximum context length), it is combinatorially large and lacks inherent geometric structure suitable for quantitative analysis of convergence, divergence or semantic drift. To measure such variations, we construct a continuous representation space through embedding, as described in the following subsection.

3.2 Representation Space and Embedding Function

To enable quantitative analysis of semantic similarity, we construct a continuous **representation space** \mathcal{E} by embedding textual objects into a geometric space where distances and similarities can be measured.

Let $\phi : \mathcal{A} \rightarrow \mathbb{R}^d$ denote an **embedding function** that maps each object $a \in \mathcal{A}$ to a dense vector representation $\phi(a) \in \mathbb{R}^d$ in a d -dimensional Euclidean space. To ensure that similarity measurements depend solely on directional alignment (not magnitude), we apply ℓ_2 -normalization to all embeddings. Let $\psi : \mathcal{A} \rightarrow \mathbb{S}^{d-1}$ denote the **normalized embedding function** defined as:

$$\psi(a) = \frac{\phi(a)}{\|\phi(a)\|_2}, \quad (1)$$

where $\mathbb{S}^{d-1} = \{e \in \mathbb{R}^d : \|e\|_2 = 1\}$ is the $(d - 1)$ -dimensional unit hypersphere. We define the **representation space** as:

$$\mathcal{E} = \{\psi(a) \mid a \in \mathcal{A}\} \subset \mathbb{S}^{d-1}. \quad (2)$$

Each object a is thus represented by a unit vector $e = \psi(a) \in \mathcal{E}$.

Model-agnostic framework. The framework presented above is **embedding-model agnostic**: any sentence encoder that maps text to dense vectors can instantiate ϕ and our analysis applies regardless of the specific model choice.

Implementation choice. For this work, we instantiate ϕ using the Xenova/paraphrase-mpnet-base-v2 model, a pretrained transformer encoder with $d = 768$ dimensions. This model was chosen for three practical reasons:

1. It is trained on sentence pairs with human-labeled paraphrase relations, ensuring that geometric proximity corresponds to semantic similarity.
2. It offers a balanced trade-off between expressiveness and dimensionality, allowing fine-grained distinctions while remaining computationally efficient.
3. The Xenova implementation provides a reproducible and locally executable inference pipeline, facilitating controlled experimentation without external API dependencies.

The normalized representation space $\mathcal{E} \subset \mathbb{S}^{767}$ thus forms the manifold on which all further measurements (distances, similarities and clustering) are defined.

3.3 Similarity Metric

Within the representation space \mathcal{E} , each object $a \in \mathcal{A}$ is represented by its normalized embedding $e = \psi(a) \in \mathcal{E} \subset \mathbb{S}^{d-1}$. We define the model-based similarity function as

$$s^{(m)} : \mathbb{S}^{d-1} \times \mathbb{S}^{d-1} \rightarrow [-1, 1], \quad s^{(m)}(e_1, e_2) = \langle e_1, e_2 \rangle. \quad (3)$$

Since all elements of \mathcal{E} are unit vectors (i.e., $\|e\|_2 = 1$ for all $e \in \mathcal{E}$), the inner product $\langle e_1, e_2 \rangle$ directly equals the cosine of the angle between them, providing a normalized measure of semantic proximity.

4 Similarity Distribution and Human Alignment

On a standard high-dimensional unit sphere \mathbb{S}^{d-1} , two random vectors u, v drawn uniformly from the surface tend to be nearly orthogonal as the dimension increases. Formally, let X be uniformly distributed on \mathbb{S}^{d-1} and let $f(X) = \langle X, v \rangle$ for a fixed $v \in \mathbb{S}^{d-1}$. By Lévy's concentration inequality (see [12] for a modern treatment), for any $t > 0$,

$$\mathbb{P}(|f(X) - \mathbb{E}[f(X)]| > t) \leq 2e^{-cnt^2}, \quad (4)$$

where $c > 0$ is an absolute constant and $n = d - 1$ is the dimension of the sphere. Since $\mathbb{E}[f(X)] = 0$ for the uniform distribution, the inner product $\langle u, v \rangle$ concentrates exponentially fast around 0 as $d \rightarrow \infty$. In such isotropic settings, the similarity distribution is symmetric and sharply peaked near zero.

However, the semantic embedding space induced by a pretrained language model such as paraphrase-mpnet-base-v2 diverges from this theoretical isotropy. Because the model was trained on non-uniform pairs of semantically related sentences, the embeddings are not uniformly distributed over the hypersphere but rather cluster around a dominant mean direction in \mathbb{R}^d . This induces a strong *anisotropy* of the embedding manifold, where most vectors share a large positive cosine with the mean embedding vector. As formalized by [3], good representation learning requires balancing two properties: *alignment* (similar points should be close) and *uniformity* (embeddings should be distributed uniformly on the unit sphere). The observed concentration violates the uniformity property, indicating that the pretrained model prioritizes alignment over uniform distribution. This trade-off is typical of contrastively trained embeddings. Empirically, the distribution of $s^{(m)}(e_1, e_2)$ is concentrated around 0.8, in stark contrast with the isotropic baseline centered at 0.

In the following subsections, we evaluate how well $s^{(m)}$ aligns with human semantic judgments through quantitative metrics (§4.1) and visualization (§4.3).

4.1 Quantitative Metrics for Model-Human Alignment

To quantitatively assess how well $s^{(m)}$ aligns with human semantic judgments, we use the **MTEB STS Benchmark (STS-train)** dataset. This dataset contains pairs of textual objects $(a_1, a_2) \in \mathcal{A} \times \mathcal{A}$ annotated with normalized human similarity scores $s^{(h)}(a_1, a_2) \in [0, 1]$, rescaled from the original 0–5 range.

For each pair (a_1, a_2) , we compute their normalized embeddings $e_1 = \psi(a_1)$ and $e_2 = \psi(a_2)$ in the representation space \mathcal{E} . We then evaluate the model-based similarity $s^{(m)}(e_1, e_2)$ and compare it to the human judgment $s^{(h)}(a_1, a_2)$.

We evaluate their alignment using complementary metrics, each capturing a distinct aspect of correlation or calibration:

- **Root Mean Squared Error (RMSE):**

$$\text{RMSE} = \sqrt{\frac{1}{N} \sum_{k=1}^N (s^{(m)}(e_1^k, e_2^k) - s^{(h)}(e_1^k, e_2^k))^2} \in [0, 1].$$

Measures the average magnitude of deviation between model and human similarities, penalizing large discrepancies more strongly. Lower RMSE indicates better agreement (RMSE = 0 means perfect match; RMSE = 1 indicates maximum deviation).

- **Mean Bias Error (MBE):**

$$\text{MBE} = \frac{1}{N} \sum_{k=1}^N (s^{(m)}(e_1^k, e_2^k) - s^{(h)}(e_1^k, e_2^k)) \in [-1, 1].$$

Quantifies systematic bias: positive when the model tends to overestimate human similarity, negative when it underestimates. MBE = 0 indicates no systematic bias; $|\text{MBE}|$ close to 1 indicates severe consistent over- or under-estimation.

- **Expected Calibration Error (ECE):** This metric evaluates the degree to which model similarity scores are statistically calibrated to human perception. We partition the similarity range $[0, 1]$ into B bins, where B_b denotes the set of sample pairs in bin b . For each bin, we compute:

- $\text{acc}(B_b)$: the average human similarity score (*accuracy*, i.e., ground truth) within that bin
- $\text{conf}(B_b)$: the average model similarity score (*confidence*, i.e., predicted value) within that bin

The ECE is then computed as the weighted average absolute deviation:

$$\text{ECE} = \sum_{b=1}^B \frac{|B_b|}{N} |\text{acc}(B_b) - \text{conf}(B_b)| \in [0, 1].$$

Lower ECE values indicate better calibration (ECE = 0 means perfect calibration; ECE = 1 indicates maximum miscalibration).

- **Pearson Correlation Coefficient (r):**

$$r = \frac{\text{Cov}(s^{(m)}, s^{(h)})}{\sigma_{(m)} \sigma_{(h)}} \in [-1, 1],$$

where $\text{Cov}(s^{(m)}, s^{(h)})$ is the covariance between model and human similarity scores, $\sigma_{(m)}$ is the standard deviation of model scores and $\sigma_{(h)}$ is the standard deviation of human scores. Explicitly, this can be computed as:

$$r = \frac{\sum_{k=1}^N (s_k^{(m)} - \bar{s}^{(m)})(s_k^{(h)} - \bar{s}^{(h)})}{\sqrt{\sum_{k=1}^N (s_k^{(m)} - \bar{s}^{(m)})^2} \sqrt{\sum_{k=1}^N (s_k^{(h)} - \bar{s}^{(h)})^2}},$$

where $\bar{s}^{(m)}$ is the mean of model scores, $\bar{s}^{(h)}$ is the mean of human scores and N is the total number of pairs. This metric captures the strength of *linear* dependence between model and human similarities. $r = 1$ indicates perfect positive linear correlation, $r = -1$ indicates perfect negative linear correlation and $r = 0$ indicates no linear correlation. Values closer to ± 1 indicate stronger linear alignment.

- **Spearman Rank Correlation (ρ):**

$$\rho = r_{\text{Pearson}}(\text{rank}(s^{(m)}), \text{rank}(s^{(h)})) \in [-1, 1],$$

where $\text{rank}(s^{(m)})$ assigns each model similarity score its position when all N scores are sorted in ascending order and similarly for $\text{rank}(s^{(h)})$. The function $r_{\text{Pearson}}(\cdot, \cdot)$ denotes the Pearson correlation coefficient applied to these rank vectors. This metric measures the *monotonic* alignment between the two orderings, independently of scale. $\rho = 1$ indicates perfect monotonic agreement (rankings perfectly aligned), $\rho = -1$ indicates perfect monotonic disagreement (rankings perfectly reversed) and $\rho = 0$ indicates no monotonic relationship. Values closer to ± 1 indicate stronger monotonic alignment.

Quantitatively, the results obtained on the STS-train dataset are:

$$\text{RMSE} = 0.1702, \quad \text{MBE} = 0.0789, \quad \text{ECE} = 0.0797, \quad r = 0.8576, \quad \rho = 0.8430. \quad (5)$$

These metrics reveal several key properties of the embedding space. The **RMSE of 0.17** indicates a moderate average deviation between model and human similarities, suggesting reasonable overall agreement with some residual discrepancies. The **positive MBE of 0.079** shows a systematic tendency for the model to overestimate semantic similarity compared to human judgments. This is a characteristic feature of dense embedding spaces where related concepts cluster more tightly than human perception suggests. The **ECE of 0.080** quantifies the calibration gap: the model's similarity scores are not perfectly aligned with the empirical frequency of human agreement, reflecting the need for recalibration to achieve probabilistic consistency. The **strong correlation values** ($r = 0.86$ and $\rho = 0.84$) confirm that despite these biases, the model captures the underlying rank order and linear structure of human semantic similarity judgments. Together, these results indicate that the embedding space preserves semantic relationships effectively while exhibiting systematic geometric biases, specifically anisotropic concentration of embeddings, that lead to consistent overestimation and miscalibration.

4.2 High-Confidence Similarity Threshold

To obtain a reliable decision boundary for semantic similarity, we introduce the **High-Confidence Similarity Threshold** $\tau_{\text{HCS}}(s)$, a data-driven value derived from human-judged highly similar pairs. This threshold provides a statistically principled criterion for determining when two sentences can be considered semantically similar with high confidence. Importantly, this concept is independent of any particular similarity measure and can be applied to any similarity function.

Definition. For a given similarity function s (such as the raw cosine similarity $s^{(m)}$ or any other similarity function), the threshold is computed as:

$$\tau_{\text{HCS}}(s) = Q_{0.05}(s \mid s^{(h)} > 0.9) \quad (6)$$

that is, the 5% quantile of the similarity scores s among sentence pairs with high human similarity ($s^{(h)} > 0.9$). The confidence level $\alpha = 0.05$ is a standard choice, though it can be adjusted based on application requirements.

Interpretation. This definition is meaningful for three key reasons. First, the threshold is grounded in human judgments of semantic similarity rather than arbitrary choice. Second, it captures the lower bound of similarity scores for similar sentences as judged by humans. Third, it provides a direct probabilistic guarantee: at least 95% of truly similar pairs (those with $s^{(h)} > 0.9$) lie above this threshold.

Statistical justification. By construction, the threshold satisfies:

$$\mathbb{P}(s \geq \tau_{\text{HCS}}(s) \mid s^{(h)} > 0.9) \geq 0.95 \quad (7)$$

This conditional probability allows us to make reliable decisions: if a pair exceeds the threshold, it is likely to belong to the high-similarity group as defined by human raters.

Decision criterion. Any pair with similarity $s \geq \tau_{\text{HCS}}(s)$ can be considered semantically similar with high confidence.

For the raw cosine similarity, we denote:

$$\tau_{\text{HCS}}^{(m)} = \tau_{\text{HCS}}(s^{(m)}) \approx 0.72 \quad (8)$$

4.3 Visualization of Similarity Distributions

Beyond these numerical indicators, we visualize the distributions and relationships between $s^{(m)}$ and $s^{(h)}$ using density estimation techniques.

To compare model similarities with human similarity judgments, we estimate their respective continuous distributions using *Kernel Density Estimation (KDE)*. Each observed value contributes a Gaussian “bump” to the overall density, producing a smooth, non-parametric approximation of the underlying probability function:

$$\hat{f}_h(x) = \frac{1}{nh\sqrt{2\pi}} \sum_{i=1}^n e^{-\frac{1}{2}\left(\frac{x-x_i}{h}\right)^2}, \quad h = 1.06 \hat{\sigma} n^{-1/5}. \quad (9)$$

Silverman’s rule [13] selects the optimal bandwidth h , balancing smoothness and resolution. We compute separate densities for human scores and model similarities, $\hat{f}_H(x)$ and $\hat{f}_S(x)$ and plot them over $[0, 1]$. Alignment between both curves indicates good agreement, while systematic shifts reveal under- or over-confidence in the model’s similarity predictions. Additionally, both visualizations include a vertical green line marking the high-confidence similarity threshold $\tau_{\text{HCS}}^{(m)}$ (defined in §4.2), which serves as a data-driven decision boundary for determining when two sentences can be considered semantically similar with high confidence.

In addition to that, we also compute joint density heatmaps. To evaluate the relationship between human similarity judgments and model predictions, we estimate their joint density over the $[0, 1]^2$ space. The domain is divided into a regular grid of bins and each cell’s density $\rho_{ij} = N_{ij}/(n \Delta x \Delta y)$ reflects the concentration of pairs (h_i, s_i) . A 2D Gaussian smoothing kernel can be applied to obtain a continuous density field $\tilde{\rho}(x, y)$, from which iso-density contours and a color intensity map are derived. The diagonal $y = x$ represents perfect alignment, where model similarities equal human scores. High density concentrated along this diagonal indicates strong agreement, while systematic deviations above or below it reveal over- or under-confidence and vertical dispersion signals inconsistency in the model’s predictions.

Figure 1 shows model similarities concentrated in a narrow high-value band, while human scores spread across the full $[0, 1]$ range. This concentration reflects the anisotropic geometry of pre-trained embeddings. The green vertical line at $\tau_{\text{HCS}}^{(m)}$ marks the threshold derived from high-confidence human judgments.

Figure 2 shows the joint density $\tilde{\rho}(s^{(h)}, s^{(m)})$ as a heatmap. The density mass lies above the diagonal $y = x$, confirming systematic overestimation. For intermediate human scores ($s^{(h)} \in [0.3, 0.7]$), model predictions compress into a narrow band around 0.8, while dissimilar pairs ($s^{(h)} < 0.3$) show better correspondence.

These visualizations expose a fundamental calibration gap: the model’s cosine similarity $s^{(m)}(e_1, e_2)$ does not align with human semantic judgments $s^{(h)}(e_1, e_2)$, both in terms of distribution shape (concentration vs. spread) and pointwise correspondence (systematic overestimation). This raises a natural question: *Can we recalibrate or transform the model’s similarity function to improve its correlation with human semantic judgments?* This question is investigated in the following section.

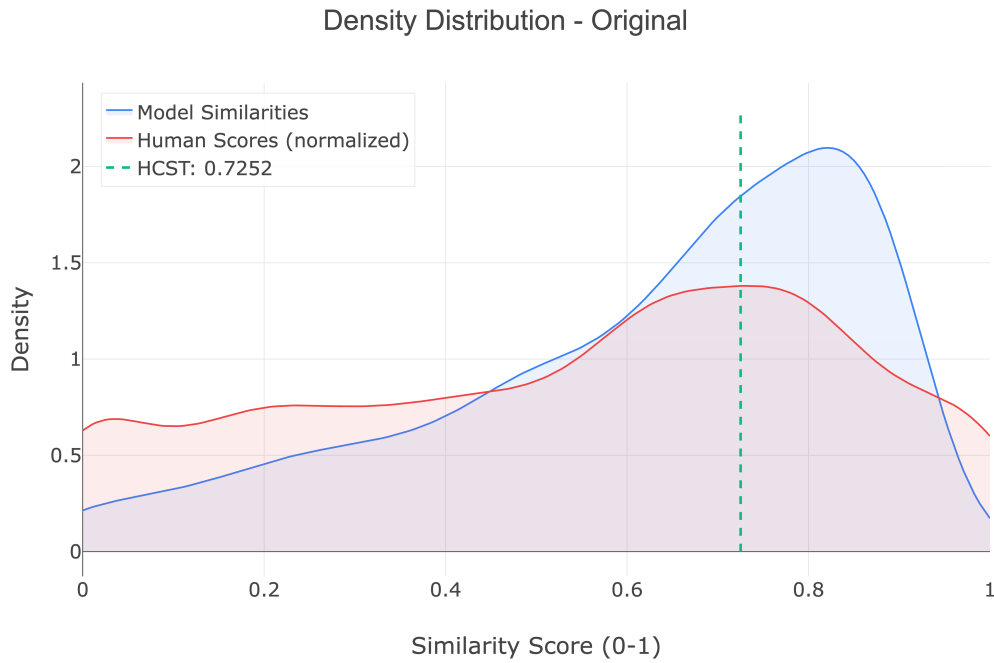


Figure 1: Density plot (KDE) of original (uncalibrated) cosine similarity versus human similarity scores.

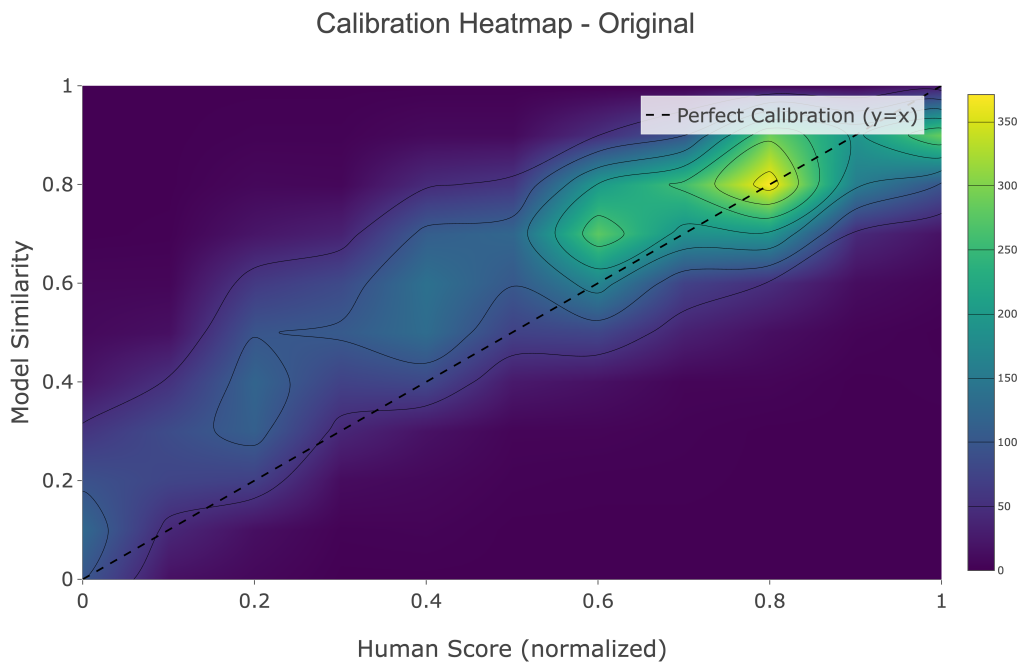


Figure 2: Heatmap of original (uncalibrated) cosine similarity versus human similarity scores.

5 Calibration of Semantic Similarity

The visualizations in Section 4.3 reveal systematic bias in the model’s similarity predictions: $s^{(m)}$ consistently overestimates human judgments $s^{(h)}$ and exhibits compressed variance. Calibration provides a post-processing mechanism to correct these distributional and pointwise misalignments.

Formally, calibration seeks a transformation function $g : [-1, 1] \rightarrow \mathbb{R}$ such that the calibrated similarity

$$\tilde{s}(e_1, e_2) = g(s^{(m)}(e_1, e_2)) \quad (10)$$

better aligns with human similarity judgments $s^{(h)}(e_1, e_2)$.

5.1 Overview of Calibration Methods

We evaluate several calibration functions that map cosine similarity to human-aligned scores, each varying in parametric flexibility and nonlinearity.

Linear regression fits a simple affine transformation $\tilde{s}(x) = ax + b$, providing a global scaling and shift but unable to capture nonlinear patterns.

Isotonic regression learns a monotonic, piecewise-constant mapping that adapts locally to the data without assuming a functional form, allowing flexible nonlinear calibration while preserving rank ordering.

Sigmoid mapping applies a logistic curve $\tilde{s}(x) = 1/(1 + e^{-a(x-b)})$, modeling smooth saturation at similarity extremes.

Polynomial transformations (degrees 2, 3 and 4) fit $\tilde{s}(x) = \sum_{i=0}^n a_i x^i$, offering increasing flexibility to model curvature, though higher degrees may introduce unwanted oscillations.

Beta distribution calibration uses a beta CDF parameterized by shape α and β , suited for bounded, skewed distributions but prone to instability when assumptions mismatch the data.

Visualizations of each calibration method’s effect on the similarity distribution are provided in Appendix A.

5.2 Results

Table 1 presents the performance comparison of all calibration methods against the original (un-calibrated) cosine similarity using correlation metrics. Percentage changes relative to the original baseline are shown for reference.

Method	RMSE	MBE	ECE	Pearson r	Spearman ρ
Original	0.1702	0.0789	0.0797	0.8576	0.8430
Linear	0.1506 $\downarrow 11.5\%$	0.0000 $\downarrow 100.0\%$	0.0222 $\downarrow 72.1\%$	$0.8576 \pm 0.0\%$	$0.8430 \pm 0.0\%$
Isotonic	0.1411 $\downarrow 17.1\%$	0.0000 $\downarrow 100.0\%$	0.0000 $\downarrow 99.9\%$	0.8764 $\uparrow 2.2\%$	0.8563 $\uparrow 1.6\%$
Sigmoid	0.3192 $\uparrow 87.6\%$	0.2604 $\uparrow 230.2\%$	0.2604 $\uparrow 226.7\%$	0.8182 $\downarrow 4.6\%$	$0.8430 \pm 0.0\%$
Beta	0.5168 $\uparrow 203.6\%$	-0.3011 $\uparrow 281.8\%$	0.4243 $\uparrow 432.3\%$	-0.8266 $\downarrow 196.4\%$	-0.8246 $\downarrow 197.8\%$
Polynomial-2	0.1474 $\downarrow 13.4\%$	0.0004 $\downarrow 99.5\%$	0.0095 $\downarrow 88.1\%$	0.8641 $\uparrow 0.8\%$	$0.8430 \pm 0.0\%$
Polynomial-3	0.1472 $\downarrow 13.5\%$	0.0000 $\downarrow 100.0\%$	0.0057 $\downarrow 92.8\%$	0.8644 $\uparrow 0.8\%$	$0.8430 \pm 0.0\%$
Polynomial-4	0.1472 $\downarrow 13.5\%$	-0.0000 $\downarrow 100.0\%$	0.0058 $\downarrow 92.7\%$	0.8645 $\uparrow 0.8\%$	$0.8430 \pm 0.0\%$

Table 1: Performance comparison of calibration methods with percentage changes relative to the original baseline. For RMSE, MBE and ECE, lower is better (green \downarrow); for Pearson and Spearman, higher is better (green \uparrow).

Isotonic regression achieves the strongest monotonic correlation (Spearman $\rho = 0.8563$) and lowest calibration error (ECE = 0.0000), with perfect elimination of mean bias (MBE = 0.0000) and a 17.1% reduction in RMSE compared to the original baseline. This defines our *calibrated similarity function*

$$\tilde{s} : \mathbb{S}^{d-1} \times \mathbb{S}^{d-1} \rightarrow \mathbb{R}, \quad \tilde{s} = f_{\text{isotonic}} \circ s^{(m)} \quad (11)$$

used throughout the analysis. In practice, since we align with human similarity scores in $[0, 1]$, calibrated outputs are clamped to this interval.

6 Structural Invariants of Isotonic Calibration

Beyond empirical performance, isotonic calibration possesses important theoretical properties that guarantee preservation of geometric structure. These invariants are central to our argument that calibration restores interpretability without compromising the validity of similarity-based analysis.

6.1 Order Preservation

Proposition (Order preservation under isotonic calibration). For any $x, y, z \in \mathbb{S}^{d-1}$:

$$s(x, y) \geq s(x, z) \implies \tilde{s}(x, y) \geq \tilde{s}(x, z). \quad (12)$$

Isotonic calibration preserves all ordering relations induced by cosine similarity. It may introduce additional ties but can never invert the order of two similarities.

Proof. Since f_{isotonic} is monotonically non-decreasing, for any $a, b \in [-1, 1]$, $a \geq b \implies f_{\text{isotonic}}(a) \geq f_{\text{isotonic}}(b)$. Applying this to $a = s(x, y)$ and $b = s(x, z)$:

$$\tilde{s}(x, y) = f_{\text{isotonic}}(s(x, y)) \geq f_{\text{isotonic}}(s(x, z)) = \tilde{s}(x, z). \quad \square$$

This fundamental property yields several important consequences for geometric analysis.

6.2 Geometric Invariants

Corollary 1 (Angular order preservation). On the unit sphere, cosine similarity relates to geodesic angle by $s(x, y) = \cos(\theta(x, y))$, where $\theta(x, y) \in [0, \pi]$. Since \cos is strictly decreasing on $[0, \pi]$:

$$\theta(x, y) \leq \theta(x, z) \implies s(x, y) \geq s(x, z) \implies \tilde{s}(x, y) \geq \tilde{s}(x, z).$$

Isotonic calibration does not modify the angular ordering of points around any center; it can only render multiple angles indistinguishable at the similarity level.

Corollary 2 (Nearest neighbor preservation). Let $x \in \mathbb{S}^{d-1}$ and $Y = \{y_1, \dots, y_n\} \subset \mathbb{S}^{d-1}$ be a finite set of candidates. If $y^* \in Y$ is a nearest neighbor of x under raw similarity, i.e., $s(x, y^*) \geq s(x, y_i)$ for all i , then:

$$\tilde{s}(x, y^*) \geq \tilde{s}(x, y_i) \quad \forall i.$$

Every nearest neighbor under s remains a nearest neighbor under \tilde{s} . Isotonic calibration may enlarge the set of tied neighbors but can never exclude a true nearest neighbor.

Corollary 3 (Threshold graph invariance). Let $X = \{x_1, \dots, x_n\} \subset \mathbb{S}^{d-1}$ and define the threshold similarity graph $E_\tau = \{(i, j) : s(x_i, x_j) \geq \tau\}$ for threshold $\tau \in [-1, 1]$. For the calibrated threshold $\tilde{\tau} = f_{\text{isotonic}}(\tau)$:

$$s(x_i, x_j) \geq \tau \implies \tilde{s}(x_i, x_j) = f_{\text{isotonic}}(s(x_i, x_j)) \geq f_{\text{isotonic}}(\tau) = \tilde{\tau},$$

which implies $E_\tau \subseteq \tilde{E}_{\tilde{\tau}}$. Isotonic calibration never destroys connections defined by a similarity threshold; it can only add edges corresponding to values made equal by the plateaus of f_{isotonic} .

6.3 Probabilistic Invariants

Corollary 4 (Invariance of high-confidence similarity thresholds). Recall that the high-confidence similarity threshold is defined as $\tau_{\text{HCS}}(s) = Q_{0.05}(s \mid s^{(h)} > 0.9)$. The calibrated threshold satisfies:

$$\tilde{\tau}_{\text{HCS}} = \tau_{\text{HCS}}(\tilde{s}) = f_{\text{isotonic}}(\tau_{\text{HCS}}(s^{(m)})).$$

Since isotonic calibration is order-preserving, any pair exceeding the raw threshold also exceeds the calibrated threshold:

$$s^{(m)} \geq \tau_{\text{HCS}}(s^{(m)}) \implies \tilde{s} \geq \tilde{\tau}_{\text{HCS}}.$$

Thus, the probabilistic guarantee $\mathbb{P}(s \geq \tau_{\text{HCS}}(s) \mid s^{(h)} > 0.9) \geq 0.95$ is preserved under calibration. \square

We can now define the high-confidence similarity threshold for the calibrated similarity:

$$\tilde{\tau}_{\text{HCS}} = \tau_{\text{HCS}}(\tilde{s}) \approx 0.65 \quad (13)$$

6.4 Summary

Isotonic calibration is an order-preserving reparameterization of cosine similarity: angular rankings, nearest-neighbor relations and threshold-based geometric structures are preserved up to the introduction of ties, but never inverted. This theoretical guarantee ensures that calibration restores interpretability without compromising the fundamental geometric properties required for downstream analysis. The calibrated similarity \tilde{s} can therefore be used as a drop-in replacement for raw cosine similarity in any application that relies on ordering, nearest-neighbor queries or threshold-based decisions.

While order preservation under monotone mappings is mathematically elementary, its consequence for embedding-space geometry has not been formalized before: it identifies the maximal class of similarity-based constructions that can be safely calibrated without altering geometric structure.

7 Evaluating Local Stability

7.1 Motivation

Even if the calibrated semantic similarity aligns well with human judgments, it remains essential to evaluate the *local stability* of the embedding function $\psi : \mathcal{A} \rightarrow \mathcal{E}$ itself. A locally stable embedding function should preserve high similarity under small linguistic perturbations: when two texts differ only slightly in form or syntax, their semantic similarity should remain consistently high. However, ψ is learned and discretized; neither its continuity nor its Lipschitz properties can be guaranteed theoretically. Our first objective is therefore empirical: to determine whether ψ behaves as *locally stable* in practice.

However, a critical methodological concern arises from our use of isotonic regression for calibration. While isotonic regression optimally preserves monotonicity and eliminates bias, it produces a *piecewise constant* (and therefore discontinuous) mapping f_{isotonic} . This raises an essential question: **does the discontinuous nature of isotonic regression degrade the local stability observed in the raw embedding space?**

To address both concerns, we conduct a dual analysis of stability:

1. **Base model stability**, evaluated on raw cosine similarity $s^{(m)}$, measures how the uncalibrated embedding function reacts to small linguistic perturbations.
2. **Calibrated stability**, evaluated on the calibrated similarity \tilde{s} , measures whether isotonic calibration preserves or degrades this local stability.

Comparing these two perspectives allows us to validate that calibration does not introduce artificial instabilities, ensuring that similarity measurements reflect genuine semantic structure rather than side effects of the calibration process.

7.2 Text Perturbation Definition

To evaluate local stability, we constructed a dedicated dataset using ChatGPT to generate pairs of sentences differing by minimal and controlled linguistic perturbations. Each pair (a_i, a'_i) was manually categorized into one of seven perturbation types, each intended to simulate a semantically minimal transformation while introducing specific syntactic or lexical variations. This approach allows for systematic testing of ψ 's local stability across controlled linguistic dimensions.

The following perturbation types were included, each illustrated with examples from the dataset:

- **DETERMINER_VARIATION:** A minimal change affecting only the determiner (the, a, this, that) without modifying the tense, structure or semantic content of the sentence. *Example:* “The cat sleeps on the sofa.” → “A cat sleeps on the sofa.”
- **TENSE_VARIATION:** A transformation that shifts the verbal tense while preserving the event described by the sentence. *Example:* “She drinks tea in the morning.” → “She drank tea in the morning.”

- **SYNONYM_SUBSTITUTION:** Replacing a lexical item (noun, verb, adjective) with a close synonym that preserves the meaning. *Example:* “He reads a book every night.” → “He reads a novel every night.”
- **LOGICAL_PARAPHRASE:** A reformulation that preserves the logical meaning of the sentence, often through active/passive alternation or structural inversion. *Example:* “The teacher explains the lesson.” → “The lesson is explained by the teacher.”
- **NOMINALIZATION:** Transforming a predicate into its nominal form (or the reverse) while keeping the meaning equivalent. *Example:* “He decided to leave early.” → “He made a decision to leave early.”
- **COREFERENCE_EXPANSION:** Replacing a pronoun with its explicit referent (or vice versa), keeping the propositional content unchanged. *Example:* “Alice lost her keys.” → “Alice lost Alice’s keys.”
- **QUANTIFIER_VARIATION:** Replacing a quantifier with another logically equivalent form (all ↔ every), without changing the truth conditions. *Example:* “All cats like to sleep.” → “Every cat likes to sleep.”

The dataset comprises 700 pairs across all categories (100 pairs per type), covering both lexical and syntactic variations. This controlled diversity allows us to examine how different perturbation types affect similarity in both the raw and calibrated embedding spaces.

7.3 Metrics and Methodology

For each pair (a_i, a'_i) , we compute their normalized embeddings $e_i = \psi(a_i)$ and $e'_i = \psi(a'_i)$ within \mathbb{S}^{d-1} . We then measure stability using two complementary similarity functions:

Base model similarity. We compute the raw cosine similarity:

$$s_i^{(m)} = s^{(m)}(e_i, e'_i) = \langle e_i, e'_i \rangle, \quad (14)$$

which measures the uncalibrated similarity between perturbed pairs.

Calibrated similarity. We also compute the calibrated similarity:

$$\tilde{s}_i = \tilde{s}(e_i, e'_i) = f_{\text{isotonic}}(s_i^{(m)}), \quad (15)$$

where f_{isotonic} denotes the isotonic regression mapping introduced in Section 5.

For each perturbation type k with N_k pairs, we compute three stability indicators:

$$\mu_k = \frac{1}{N_k} \sum_{i \in \mathcal{I}_k} s_i, \quad \sigma_k = \sqrt{\frac{1}{N_k} \sum_{i \in \mathcal{I}_k} (s_i - \mu_k)^2}, \quad r_k = \frac{1}{N_k} \sum_{i \in \mathcal{I}_k} \mathbf{1}_{\{s_i \geq \tau\}}, \quad (16)$$

where \mathcal{I}_k denotes the index set of pairs for perturbation type k and τ is the stability threshold.

Threshold selection. Rather than choosing arbitrary thresholds, we use the data-driven high-confidence similarity thresholds defined in Section 4.2:

- For base model similarity: $\tau = \tau_{\text{HCS}}^{(m)} \approx 0.72$
- For calibrated similarity: $\tau = \tilde{\tau}_{\text{HCS}} \approx 0.65$

The stability rate r_k thus measures the proportion of perturbed pairs that maintain similarity above the threshold derived from high-confidence human judgments, providing a principled criterion for local stability.

7.4 Empirical Results

Tables 2 and 3 report the local stability metrics for base model (raw cosine) and calibrated similarities, respectively. For each perturbation type, we provide the number of pairs, mean similarity, standard deviation and stability rate (proportion of pairs exceeding the corresponding threshold).

Perturbation Type	Pairs (N_i)	Mean ($\mu_{\text{base},i}$)	Std. Dev. ($\sigma_{\text{base},i}$)	Stab. Rate ($r_{\text{base},i}$)
DETERMINER VARIATION	100	0.932	0.017	1.00
TENSE VARIATION	100	0.909	0.030	1.00
SYNONYM SUBSTITUTION	100	0.853	0.060	0.95
LOGICAL PARAPHRASE	100	0.891	0.023	1.00
NOMINALIZATION	100	0.866	0.035	1.00
COREFERENCE EXPANSION	100	0.882	0.022	1.00
QUANTIFIER VARIATION	100	0.848	0.039	0.97
All types (overall)	700	0.883	0.045	0.99

Table 2: Local stability metrics using base model similarity $s^{(m)}$ (threshold $\tau_{\text{HCS}}^{(m)} = 0.72$).

Perturbation Type	Pairs (N_i)	Mean ($\mu_{\text{sim},i}$)	Std. Dev. ($\sigma_{\text{sim},i}$)	Stab. Rate ($r_{\text{sim},i}$)
DETERMINER VARIATION	100	0.926	0.054	1.00
TENSE VARIATION	100	0.868	0.069	1.00
SYNONYM SUBSTITUTION	100	0.799	0.082	0.87
LOGICAL PARAPHRASE	100	0.831	0.049	1.00
NOMINALIZATION	100	0.818	0.078	1.00
COREFERENCE EXPANSION	100	0.830	0.045	1.00
QUANTIFIER VARIATION	100	0.798	0.050	0.97
All types (overall)	700	0.839	0.075	0.98

Table 3: Local stability metrics using calibrated similarity \tilde{s} (threshold $\tilde{\tau}_{\text{HCS}} = 0.65$).

7.5 Discussion

Embedding function exhibits strong local stability. The base model analysis (Table 2) demonstrates excellent local stability with an overall stability rate of 99%. All perturbation types maintain mean similarities well above the threshold, ranging from 0.848 (QUANTIFIER_VARIATION) to 0.932 (DETERMINER_VARIATION).

Isotonic calibration introduces minimal stability degradation. Table 3 shows that isotonic calibration reduces the stability rate from 99% to 98%, a modest 1% degradation. This is attributable to the piecewise constant nature of isotonic regression: when a perturbed pair has raw cosine similarity near a discontinuity point, calibrated similarities may fall into different constant segments.

The most affected perturbation type is SYNONYM_SUBSTITUTION (stability drops from 0.95 to 0.87). This is expected: synonym substitutions produce moderate cosine similarities (mean 0.853) in a region where isotonic regression has more step discontinuities. Perturbation types with very high base similarities (DETERMINER_VARIATION: 0.932) remain perfectly stable after calibration.

Practical acceptability. Despite the theoretical discontinuity, the empirical stability rate of 98% remains highly acceptable. The 1% degradation is negligible compared to the significant gains in calibration quality (ECE reduction from 0.0797 to 0.0000).

Implications. These results validate the use of calibrated similarity \tilde{s} for geometric analysis. The embedding function exhibits strong local stability and isotonic calibration preserves this property with minimal degradation. This ensures that geometric measurements reflect genuine semantic structure rather than side effects of calibration.

8 Discussion and Applications

8.1 On the Nature of the Contribution

Although isotonic regression is a well-known calibration method, its role in this work is not algorithmic novelty but theoretical necessity. Without monotone calibration, similarity-based geometry lacks interpretability: absolute values cannot be compared across models, datasets or studies, and threshold-based decisions have no principled grounding. Our contribution is not a new algorithm, but a change in conceptual status: we argue that raw cosine similarity should not be used for absolute measurements without calibration, and we provide the theoretical framework—order preservation, structural invariance, probabilistic coherence—to support this claim. Our analysis identifies similarity calibration as the minimal transformation required to restore interpretability, while preserving the entire class of order-based geometric constructions.

8.2 Applications of Calibrated Similarity

The calibrated similarity metric enables reliable geometric analysis across several applications:

Semantic trajectory analysis. In iterative language model systems (self-refinement loops, multi-step reasoning chains, agentic systems), tracking how semantic representations evolve across iterations requires reliable similarity measurements. Calibrated similarity provides human-aligned metrics for measuring local displacement ($\tilde{s}(e_t, e_{t-1})$), global drift ($\tilde{s}(e_t, e_0)$) and trajectory coherence.

Clustering and structure detection. Clustering algorithms rely on similarity or distance metrics. When raw cosine similarities are compressed into a narrow band, distinguishing genuinely similar pairs from moderately related ones becomes difficult. Calibrated similarity expands the effective similarity range, improving cluster coherence and separation.

Similarity-based retrieval. Semantic search and document retrieval systems use similarity thresholds for relevance decisions. The high-confidence threshold $\tilde{\gamma}_{HCS}$ provides a principled, statistically grounded decision boundary derived from human judgment distributions, rather than arbitrary threshold selection.

Model evaluation and comparison. Calibrated similarity enables fair comparison of different embedding models by normalizing their similarity distributions against human judgments. This addresses the problem that different models may have systematically different similarity ranges.

8.3 Limitations

Training data dependence. The isotonic calibration is trained on the STS Benchmark, which may not perfectly represent all domains or languages. Calibration quality may degrade for domains significantly different from the training distribution.

Discontinuity effects. While local stability remains high overall, the piecewise constant nature of isotonic regression can cause discontinuities in similarity gradients. For applications requiring smooth gradients (e.g., gradient-based optimization), polynomial calibration may be preferable despite lower overall performance.

Model specificity. The calibration function f_{isotonic} is specific to the embedding model used. Different models require separate calibration, though the methodology applies uniformly.

8.4 Future Directions

Domain-specific calibration. Training calibration functions on domain-specific similarity judgments could improve performance for specialized applications (legal, medical, scientific text).

Multilingual extension. Extending calibration to multilingual embeddings and cross-lingual similarity would broaden applicability.

Smooth calibration alternatives. Investigating smooth monotonic functions (splines, monotonic neural networks) that achieve similar performance to isotonic regression while maintaining continuous gradients.

9 Conclusion

While raw cosine similarity in pretrained embeddings exhibits strong rank correlation with human judgments, anisotropy induces systematic miscalibration of absolute values, limiting their interpretability as quantitative measures. This observation does not diminish the utility of cosine similarity for ranking tasks; rather, it identifies a gap between relative ordering and absolute interpretability that matters for threshold-based decisions, clustering and cross-model comparison.

Our contribution is not to replace cosine similarity, but to restore interpretability of its absolute values through monotone calibration, without altering its ranking properties. We characterize isotonic calibration as an order-preserving reparameterization and prove that all order-based geometric constructions (angular ordering, nearest neighbors, threshold graphs, quantile-based decisions) are invariant under this transformation.

Empirically, isotonic calibration achieves near-perfect alignment with human judgments ($ECE \approx 0$, $MBE = 0$) while preserving rank correlation (Spearman $\rho = 0.856$) and local stability (98% across seven perturbation types). The calibrated similarity metric, combined with the principled high-confidence threshold $\tilde{\gamma}_{HCS} \approx 0.65$, restores interpretability for geometric analysis of embedding spaces without modifying the underlying representations.

Acknowledgments

The author thanks the creators of the MTEB STS Benchmark dataset for providing calibrated human similarity judgments and the Xenova project for providing a reproducible transformer inference pipeline.

Statements and Declarations

Competing Interests

The author declares that there are no competing financial or non-financial interests that could have influenced the work reported in this paper.

Data Availability

The experiments were conducted using the publicly available MTEB STS Benchmark dataset. Code availability will be considered following the peer-review process.

References

- [1] Kawin Ethayarajh. How contextual are contextualized word representations? comparing the geometry of bert, elmo, and gpt-2 embeddings. In *Proceedings of the 2019 Conference on Empirical Methods in Natural Language Processing*, pages 55–65, 2019.
- [2] Jianlin Su, Jiarun Cao, Weijie Liu, and Yangyiwen Ou. Whitening sentence representations for better semantics and faster retrieval, 2021.
- [3] Tongzhou Wang and Phillip Isola. Understanding contrastive representation learning through alignment and uniformity on the hypersphere. In *International Conference on Machine Learning*, pages 9929–9939, 2020.
- [4] Bianca Zadrozny and Charles Elkan. Transforming classifier scores into accurate multiclass probability estimates. In *Proceedings of the Eighth ACM SIGKDD International Conference on Knowledge Discovery and Data Mining*, pages 694–699, 2002.

- [5] Jun Gao, Di He, Xu Tan, Tao Qin, Liwei Wang, and Tie-Yan Liu. Representation degeneration problem in training natural language generation models. In *International Conference on Learning Representations*, 2019.
- [6] John Platt. Probabilistic outputs for support vector machines and comparisons to regularized likelihood methods. *Advances in Large Margin Classifiers*, 10(3):61–74, 1999.
- [7] Alexandru Niculescu-Mizil and Rich Caruana. Predicting good probabilities with supervised learning. In *Proceedings of the 22nd International Conference on Machine Learning*, pages 625–632, 2005.
- [8] Chuan Guo, Geoff Pleiss, Yu Sun, and Kilian Q. Weinberger. On calibration of modern neural networks. In *International Conference on Machine Learning*, pages 1321–1330, 2017.
- [9] Shrey Desai and Greg Durrett. Calibration of pre-trained transformers. In *Proceedings of the 2020 Conference on Empirical Methods in Natural Language Processing*, pages 295–302, 2020.
- [10] Daniel Cer, Mona Diab, Eneko Agirre, Iñigo Lopez-Gazpio, and Lucia Specia. SemEval-2017 task 1: Semantic textual similarity multilingual and crosslingual focused evaluation. In *Proceedings of the 11th International Workshop on Semantic Evaluation (SemEval-2017)*, pages 1–14, 2017.
- [11] Niklas Muennighoff, Nouamane Tazi, Loïc Magne, and Nils Reimers. Mteb: Massive text embedding benchmark. *arXiv preprint arXiv:2210.07316*, 2022.
- [12] Roman Vershynin. *High-Dimensional Probability: An Introduction with Applications in Data Science*. Cambridge University Press, 2018. Section 5.1.2, Theorem 5.1.3.
- [13] Bernard W. Silverman. *Density Estimation for Statistics and Data Analysis*. Chapman and Hall/CRC, London, 1986.

A Calibration Method Visualizations

This appendix provides visualizations for each calibration method evaluated in Section 5. For each method, we show the density plot (KDE) and heatmap comparing calibrated model similarity against human similarity scores.

A.1 Linear Regression

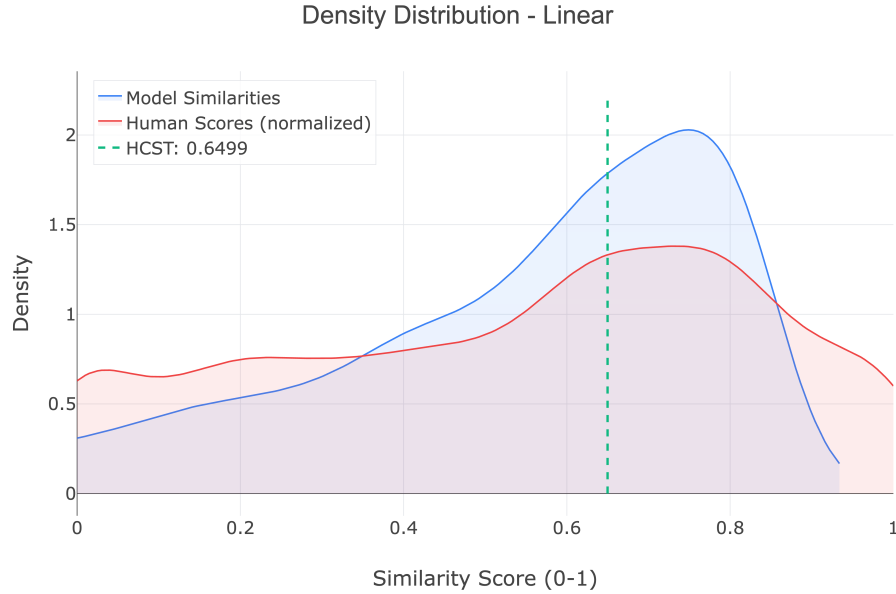


Figure 3: Linear regression calibration: density plot (KDE).

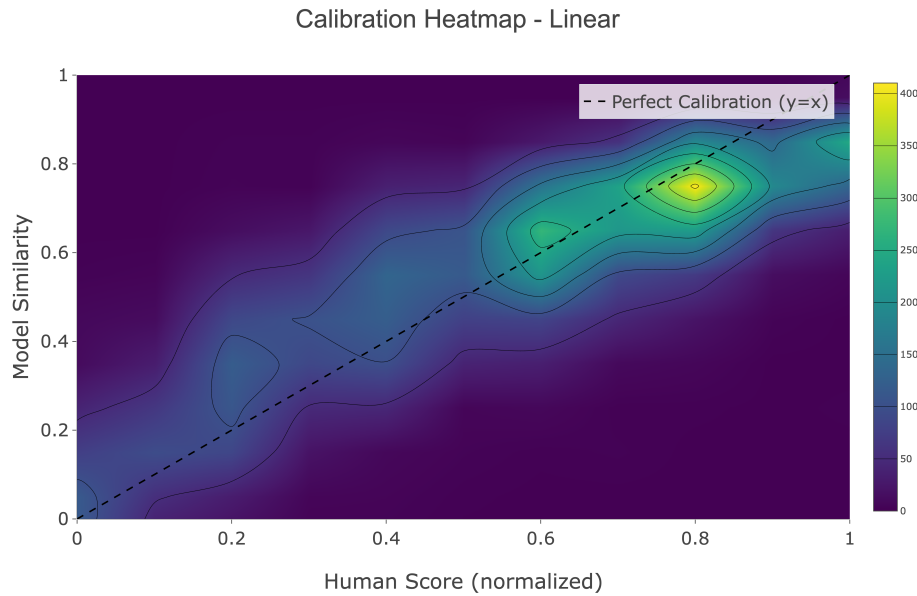


Figure 4: Linear regression calibration: heatmap.

A.2 Isotonic Regression

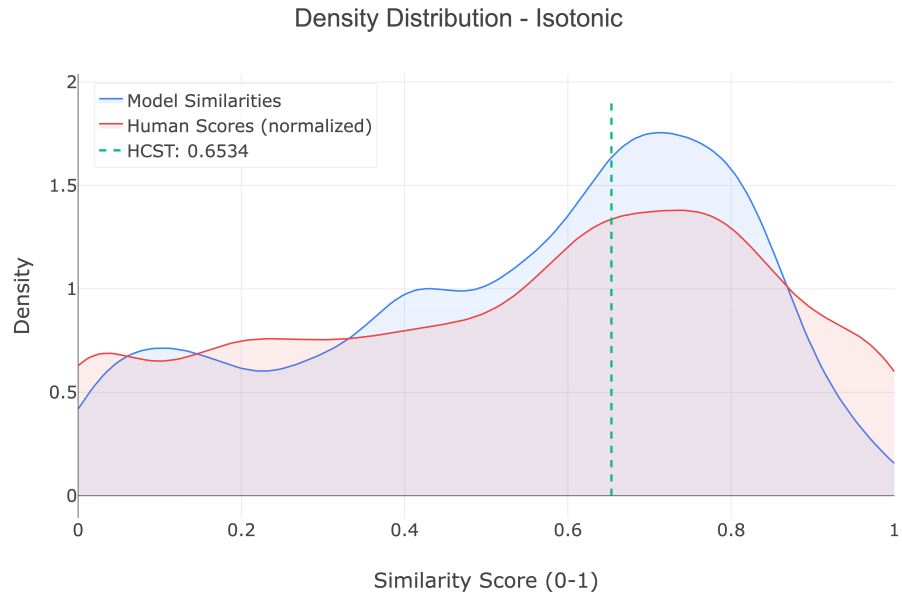


Figure 5: Isotonic regression calibration: density plot (KDE).

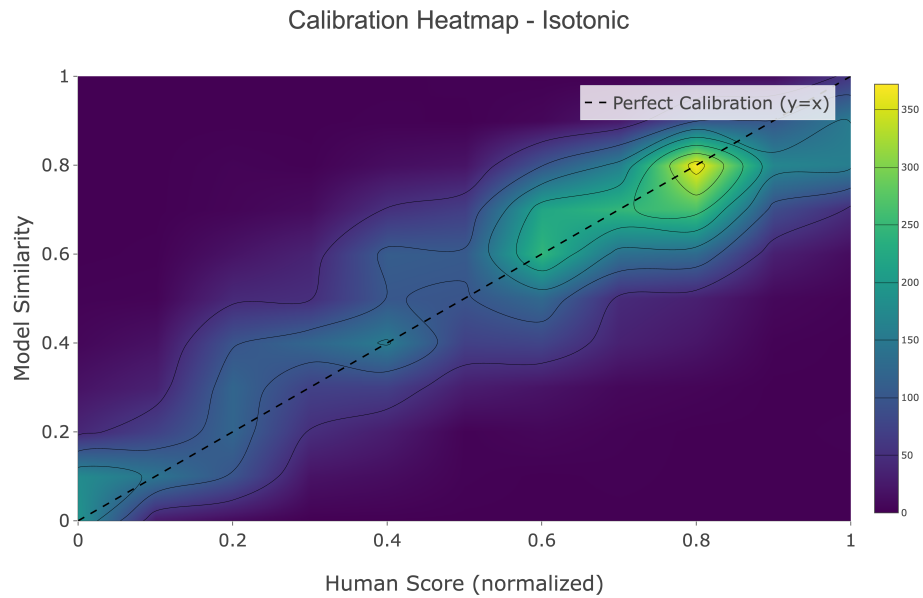


Figure 6: Isotonic regression calibration: heatmap.

A.3 Sigmoid

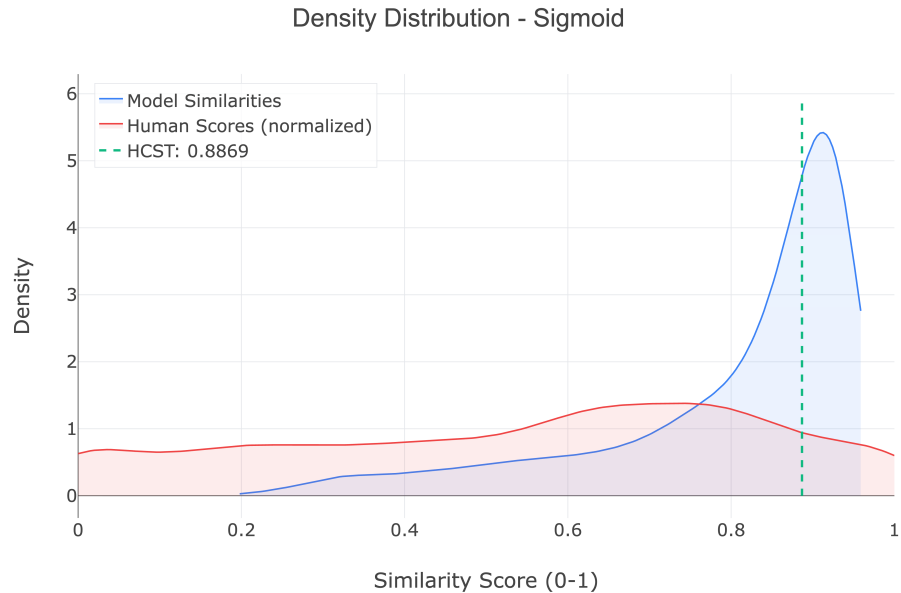


Figure 7: Sigmoid calibration: density plot (KDE).

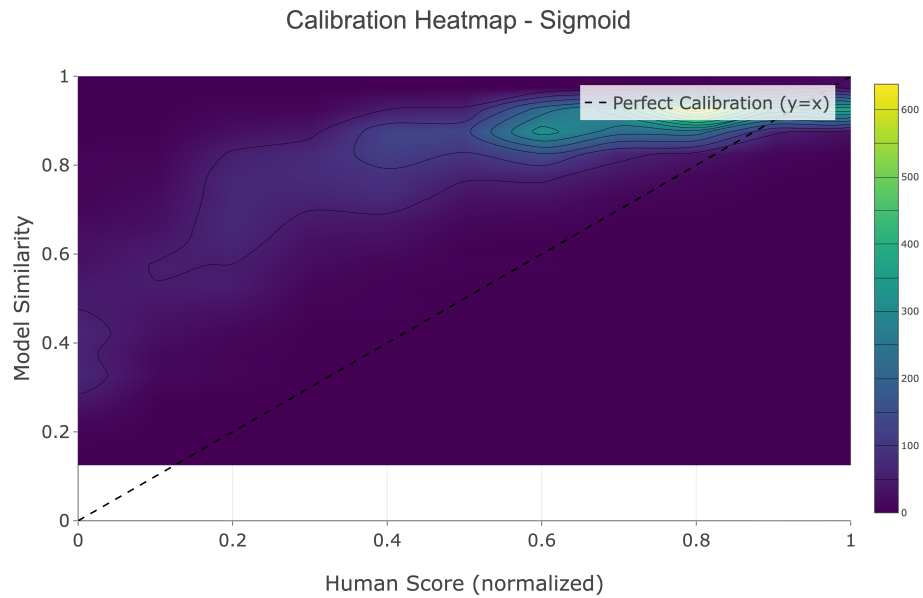


Figure 8: Sigmoid calibration: heatmap.

A.4 Polynomial (Degree 2)

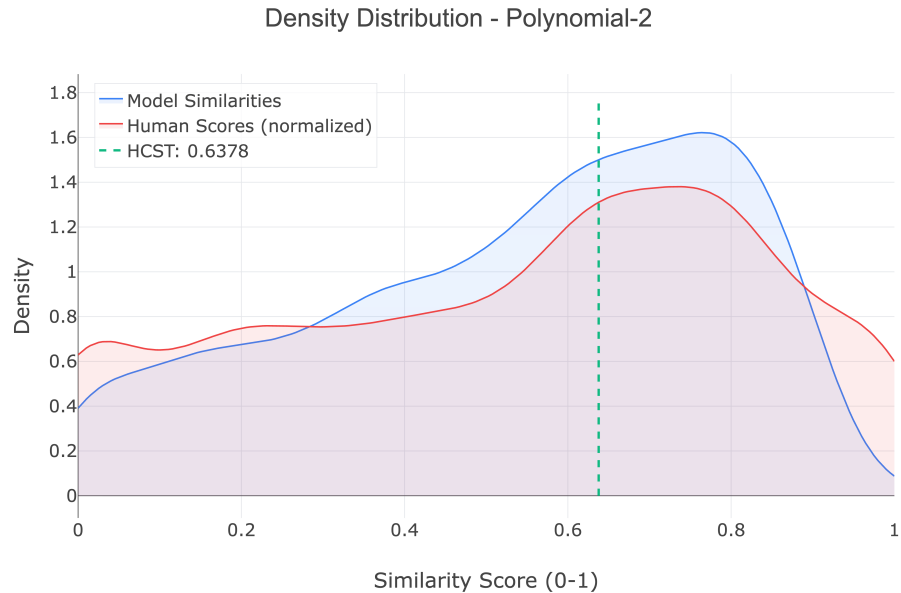


Figure 9: Polynomial degree 2 calibration: density plot (KDE).

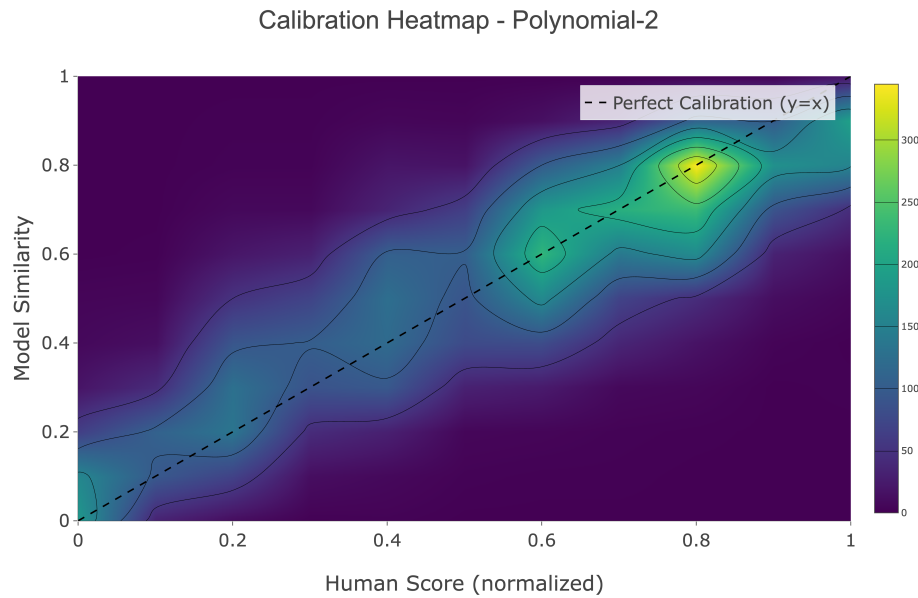


Figure 10: Polynomial degree 2 calibration: heatmap.

A.5 Polynomial (Degree 3)

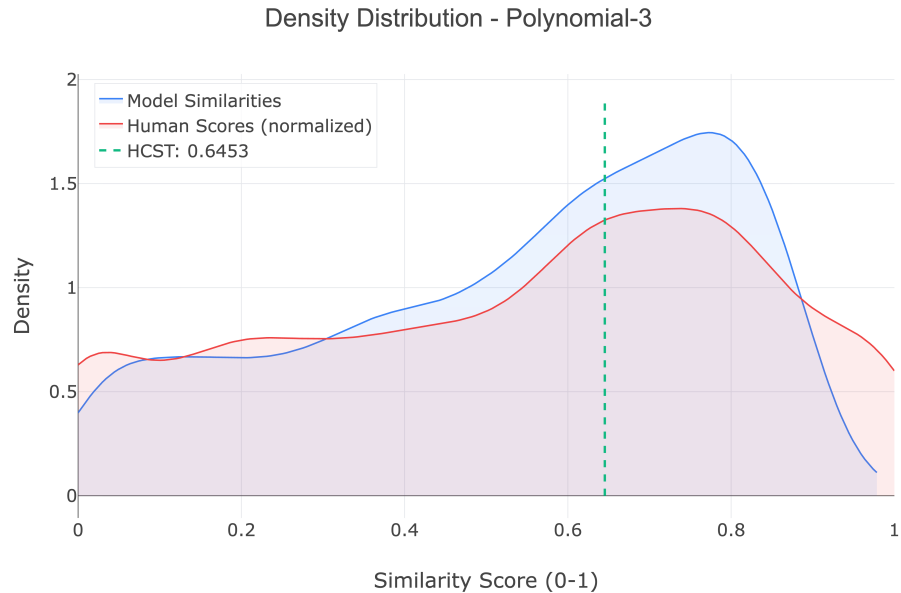


Figure 11: Polynomial degree 3 calibration: density plot (KDE).

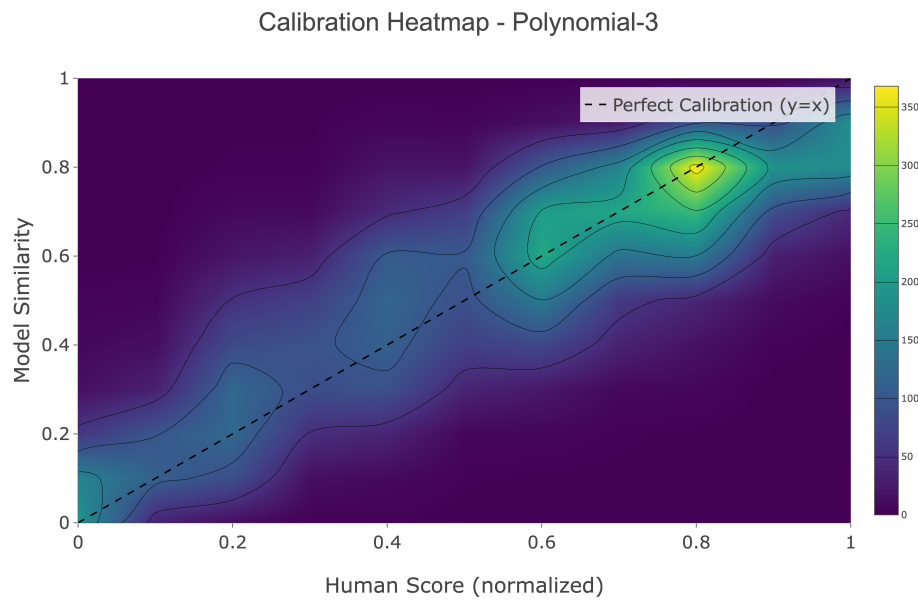


Figure 12: Polynomial degree 3 calibration: heatmap.

A.6 Polynomial (Degree 4)

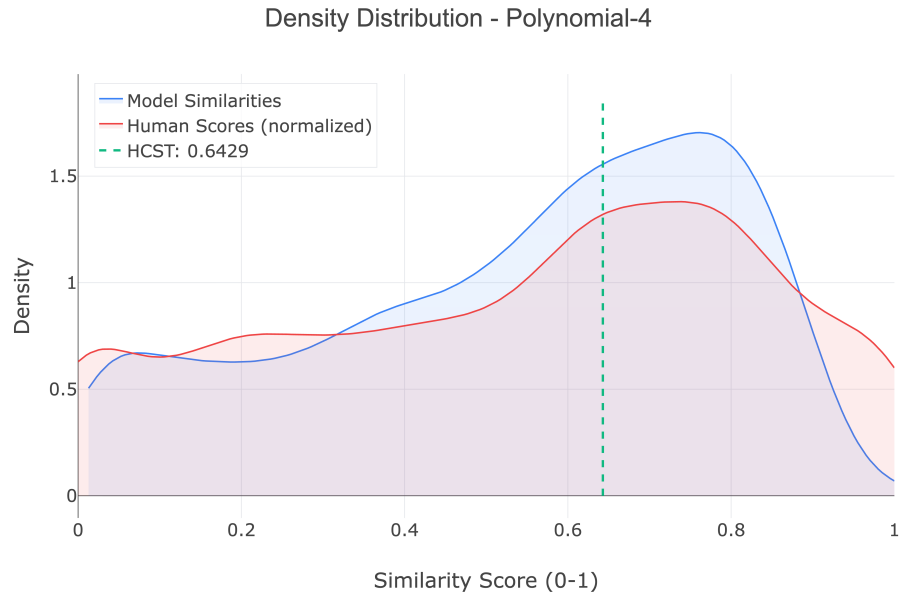


Figure 13: Polynomial degree 4 calibration: density plot (KDE).

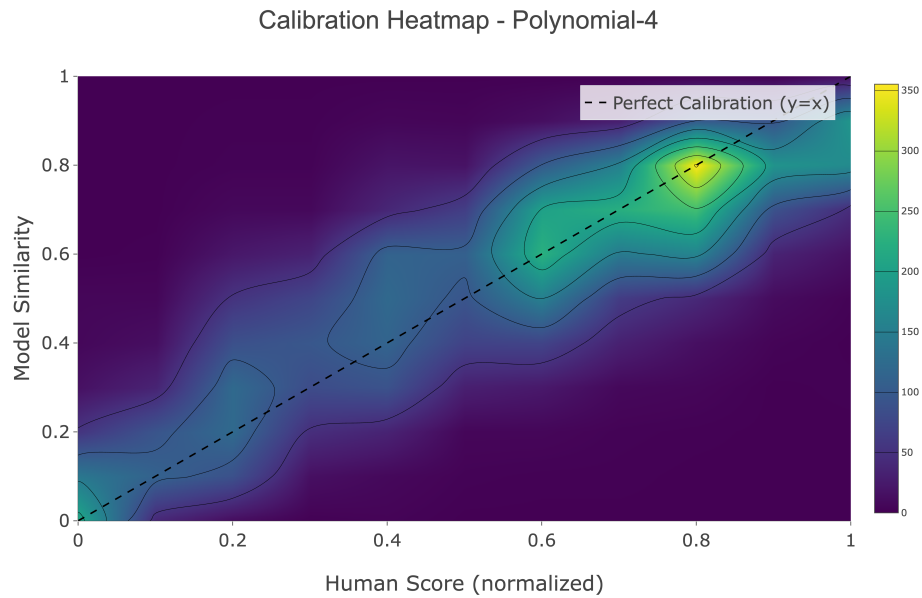


Figure 14: Polynomial degree 4 calibration: heatmap.

A.7 Beta Distribution

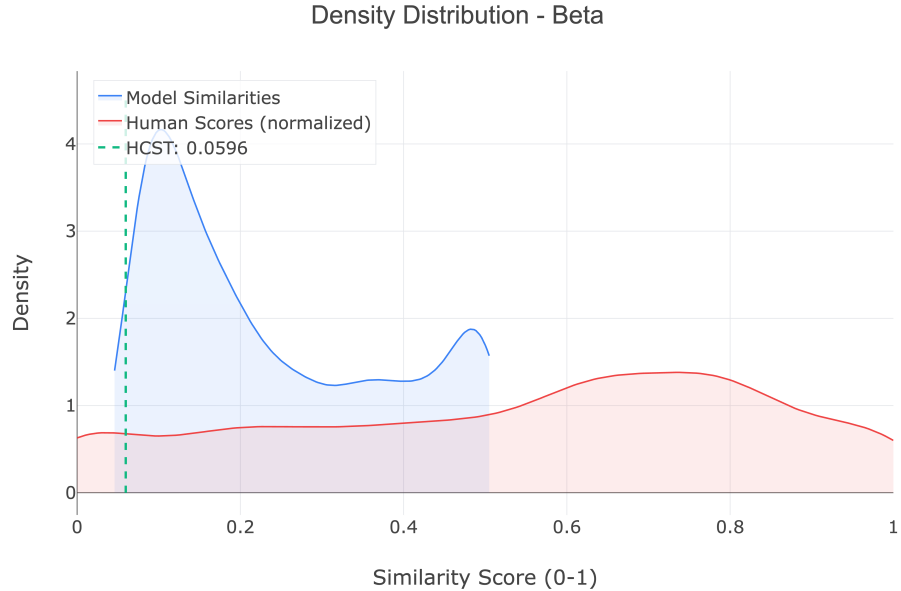


Figure 15: Beta distribution calibration: density plot (KDE).

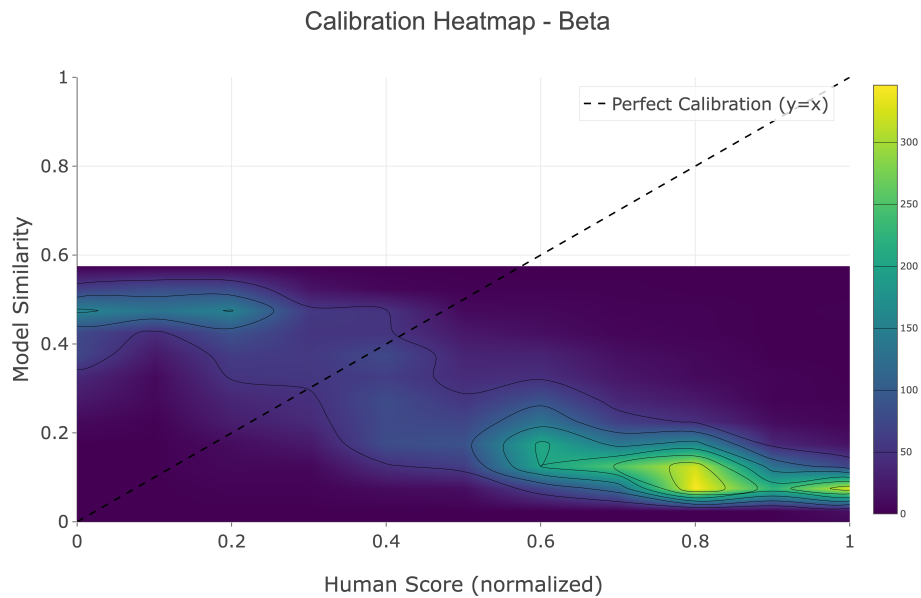


Figure 16: Beta distribution calibration: heatmap.